Optimization Design of a Novel Flux-Switching Transverse-Flux Permanent Magnet Tube Linear Motor

Dongshan Fu, Zeyu Jia, Yanliang Xu, Jinlin Gong, Frederic Gillon, Nicolas Bracikowski, Xiaojie Wu

▶ **To cite this version:**

Dongshan Fu, Zeyu Jia, Yanliang Xu, Jinlin Gong, Frederic Gillon, et al.. Optimization Design of a Novel Flux-Switching Transverse-Flux Permanent Magnet Tube Linear Motor. IEEE Transactions on Magnetics, 2021, 57 (6), pp.1-5. 10.1109/TMAG.2021.3061812 . hal-04074956

HAL Id: hal-04074956
https://hal.science/hal-04074956v1

Submitted on 17 Feb 2025

HAL is a multi-disciplinary open access archive for the deposit and dissemination of scientific research documents, whether they are published or not. The documents may come from teaching and research institutions in France or abroad, or from public or private research centers.

L'archive ouverte pluridisciplinaire **HAL**, est destinée au dépôt et à la diffusion de documents scientifiques de niveau recherche, publiés ou non, émanant des établissements d'enseignement et de recherche français ou étrangers, des laboratoires publics ou privés.

Optimization Design of a Novel Flux-Switching Transverse-Flux Permanent Magnet Tube Linear Motor

Dongshan Fu [1], Zeyu Jia[1], Yanliang Xu [2], Jinlin Gong [2], Frederic Gillon[3], Nicolas Bracikowski [4], and Xiaojie Wu[1]

[1]Jiangsu Province Laboratory of Mining Electric and Automation, China University of Mining and Technology, Xuzhou 221116, China
[2]School of Electrical Engineering, Shandong University, Jinan 250061, China
[3]Arts et Metiers ParisTech, HEI, EA 2697, L2EP, Univ. Lille, Centrale Lille, 59000 Lille, France
[4]IREENA, University of Nantes, 44600 Saint-Nazaire, France

A novel flux-switching transverse-flux permanent magnet tube linear motor (FSTFPMTLM) with oblique air-gap is proposed in this article, which combined the merits of the tube linear motor, the transverse-flux linear motor, and the switched-flux linear motor. The structure and operating principle of the FSTFPMTLM is presented first. Considering this motor has a 3-D magnetic circuit and designing the motor with high performance, this article proposes an optimization method for the FSTFPMTLM by decomposing the design of the motor into two steps to separate optimization using experimental design method. The first step is to optimize the cross-section part of the motor. After that the optimized motor is compared with the initial one by finite element method (FEM). The prototype is then manufactured and tested.

Index Terms—**Flux switching, optimization, permanent magnet (PM) tube linear motor, transverse flux.**

I. Introduction

PERMANENT magnet linear motors (PMLMs) have several advantages due to the linear direct drive with high-reliability, high-precision, high-velocity, and simple system structure [1]. Therefore, this kind of motor is greatly required in occasions where the linear motion is needed, such as rail transit, ropeless elevator, and electromagnetic launch [2]. However, the conventional PMLM is inappropriate for the applications demanding extremely long secondary core, such as ropeless elevator and rail transit, because large amounts of expensive permanent magnets (PMs) or copper windings are indispensable. The flux-switching PMLM (FSPMLM), combining the PMs and armature windings in the short part of the motor, has a lower cost and avoids long armature or long PMs as normal PMLM. The FSPMLM has the advantages of high-force density, high efficiency, and bipolar flux linkage [3]. But the magnetic field in the FSPMLM are longitudinal magnetic field that makes it difficult to relatively improve the force density [4]. The transverse-flux permanent magnetic linear motor (TFPMLM) decouples the electric circuit and the magnet circuit, providing the advantages of high-force density, design flexibility, and high reliability. Synthesizing the characteristics of the FSPMLM and the TFPMLM together, the flux-switching TFPMLM (FSTFPMLM) is put forward [1]. The magnetic circuit structure of FSTFPMLM decoupled the electric load and magnetic load. Windings and PMs are accommodated in the same part of the machine, and the other part can be made of silicon steel laminations.

In recent years, FSTFPMLMs are being researched increasingly by more and more scholars. Some novel planar FSTFPMLMs were developed in [1], [5], and [6]. But the planar one is not suitable for occasions where the system volume is strictly limited. A transverse-flux flux-reversal linear motor is proposed in [7] for the long-stroke application for the purpose of conveyance, but the PM directly contacts the air gap which is not reliable and hence this motor is not suitable for high-accuracy positioning. A novel FSTFPMLM with high force density and low-cost secondary cores was proposed in [4]; this motor has complex structure and is difficult to manufacture. Liu *et al.* [8] proposed a novel FSTFPMLM with soft magnetic composite (SMC) material which has lower permeability and complex structure. Therefore, flux-switching transverse-flux permanent magnet tube linear motor (FSTFPMTLM) with a simple structure and high force density was developed and investigated.

Moreover, the FSTFPMLM with transverse-flux structure normally suffers from the complex structure resulting from the 3-D magnetic circuit, which is usually analyzed using 3-D finite element method (FEM) with time-consuming problem [9]. Optimization design of the machine by integrating 3-D FEM features high accuracy but at unbearable cost and consuming time both in model establishment and in operation. Fast optimization design of the motor is the key to motor design, especially for the FSTFPMLM which has a 3-D magnetic circuit structure.

In this article, a novel FSTFPMTLM with a simple structure is proposed. The structure, operating principle, and advantages of the SFTFPMTLM are discussed first. Then this article proposes an optimization method for the FSTFPMTLM by decomposing the design of the motor into two steps to separate optimization using experimental design method to decrease the optimization time, and the motor is optimized and compared with the initial one. The prototype is the manufactured, and

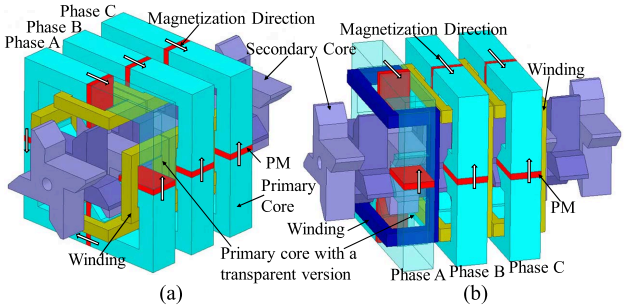

Fig. 1. Three phases of the FSTFPMTLM with two different winding structures. (a) Concentrated winding. (b) Loop-back winding.

experiments are conducted to verify the proposed model, and some conclusions are drawn.

II. Construction and Operation Principle

A. Structure of the FSTFPMTLM

The proposed novel three-phase of the FSTFPMTLM with two different winding structures are shown in Fig. 1. In the tubular-type FSTFPMTLM, it is easy to eliminate the radial electromagnetic force by ensuring a good shaft installation; and it has higher thrust-to-volume ratio and has no cut in the transverse direction so that the magnetic field is uniformly distributed along the circumferential direction [10]. The FSTFPMTLM is composed of a primary and a secondary core as the mover and stator, respectively. A primary unit is assembled by windings and tube-shaped magnetic circuit modular with salient poles. The tubular magnetic circuit module is composed of the same number of C-shaped iron cores and PMs interleaved with each other in the circumferential arrangement. Each PM and adjacent C-shaped iron cores pole are assembled as a salient pole. The distribution of the windings in the motor is flexible. One way of distributing the windings is by wounding the concentrated coil on the salient pole as shown in Fig. 1(a); the number of the coils in each phase is the same as the number of salient poles in one phase. The other way of distributing the windings is by making the coil go through the core slot of the primary unit, forming a loop-back structure as shown in Fig. 1(b); the number of coils in each phase can be the same as the number of primary units in one phase. The number of iron cores, PMs, and salient poles in the primary unit can be selected according to specific application requirements. In this article, the number is four and concentrate winding is used.

The secondary cores of the FSTFPMLM can be made of the overlying silicon steel sheet. The secondary units are arranged in sequence along the motor moving direction; the secondary units have the same structure and the adjacent secondary units are mirror symmetrical as shown in Fig. 1. It is worthy to mention that the oblique air gap is presented in this article to increase the effective area of the air gap and decrease the reluctance of the air gap.

B. Operating Principle of the FSTFPMTLM

Fig. 2 shows the magnetic flux path when the primary unit is aligned with different secondary units. The magnetic field

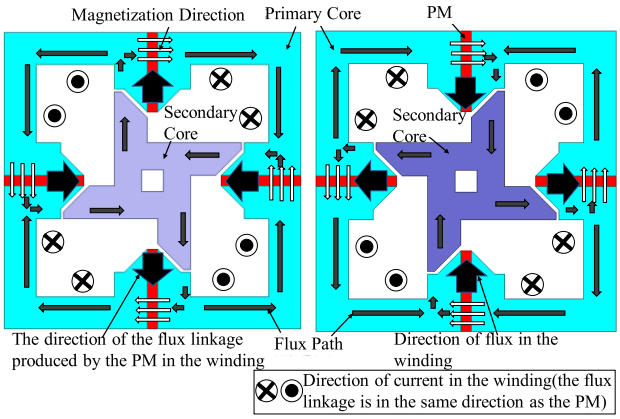

Fig. 2. Magnetic flux path.

generated by the PM passes through the primary core, air gap, secondary core, air gap, primary core, and PM to form a magnetic flux loop. When the primary unit is aligned with one secondary unit, the direction of the magnetic flux generated by the PM in the primary tooth pole is positive as shown in Fig. 2(a). The flux linkage in the windings reached the maximum positive value. While the primary unit is aligned with the adjacent secondary unit, the direction of the magnetic flux generated by the PM in the primary tooth pole is negative as shown in Fig. 2(b). The flux linkage in the windings reached the maximum negative value. With the movement of primary unit, the flux linkage in the armature winding will range from the maximum positive value to the maximum negative value synchronously. According to the fundamental principle of Faraday's law, the periodic back electromotive force (EMF) can be induced in the armature windings.

C. Structure Advantages

The proposed FSTFPMTLM has the following structural advantages.

1) *Simple Structure and Easy Assembly:* Both the primary and secondary cores of the FSTFPMLM can be made of the overlying silicon steel sheet, which is convenient to manufacture. And the secondary core has no windings and PM.
2) *Low Air Gap Reluctance:* Oblique air gap is applied to improve the motor performance which increased the effective area of the air gap.
3) *Use of Lamination:* The proposed model has a 2-D magnetic circuit in which the main flux flows transversely from the north pole to the south pole along with the iron cores, as shown in Fig. 2. In this magnetic circuit, the iron cores in the primary and secondary units can be easily fabricated using laminated silicon steel sheet that are arranged along the moving direction [11].
4) *Winding Flexible Wiring Method:* Two different ways are involved in installating the windings, which can be selected according to the working environment and structural parameters of the motor.

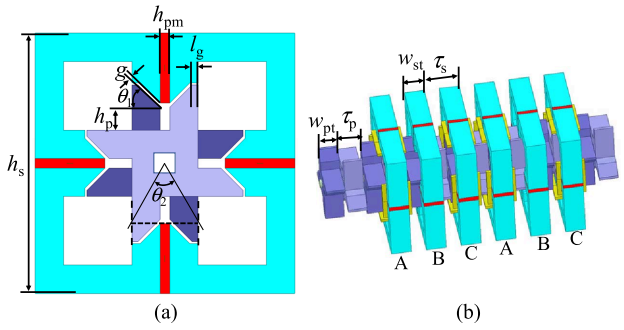

Fig. 3. Main structural parameter labels of the FSTFPMTLM. (a) Parameter labels of steel sheet. (b) Parameter labels of motor units.

TABLE I
DESIGN PARAMETERS OF FSTFPMTLM WITH INITIAL VALUE

Symbol	Quantity	Symbol	Quantity
Primary diameter h_s (mm)	80	Secondary Pole pitch τ_p (mm)	15
Air gap length g (mm)	1	Secondary unit width w_{pt} (mm)	12
Stair l_g (mm)	1	Primary pole pith τ_s (mm)	25
Secondary tooth height h_p (mm)	6	Primary unit width w_{st} (mm)	13
Magnet Magnetization h_{pm} (mm)	4	Number of primary units per phase	2
Air gap tilt angle θ_1 (°)	0	Current density J (A/mm^2)	4.5
Arc coefficient of the salient pole θ_2	0.65	Magnets: NdFeB Br=1.2T, Hc=890kA/m, Relate current I=6A	

III. MULTISTEP OPTIMIZATION OF THE FSTFPMTLM

A. Screening of Parameters and Optimization Strategies

Fig. 3 shows the main structural parameter labels of the studied FSTFPMTLM. The initial motor parameters are shown in Table I. In order to further improve the performance of the motor, the motor needs to be optimized. As mentioned above, the laminated steel plates are used to fabricate the primary and secondary units because the main flux flows in a 2-D magnetic circuit as shown in Fig. 2. And the secondary cores are of the same shape. Thus, decomposing the optimization design of the motor into two steps: the first step is the optimization of the shape of the laminated steel plates, and the related parameters are shown in Fig. 3(a). The second step is the optimization of the pole pitch and width of the primary and secondary units, and the related parameters are shown in Fig. 3(b). 2-D and 3-D finite element analyses for the first and second steps are carried out, respectively, which coupled with the experimental design method to optimize the designs of the FSTFPMTLM.

B. Optimal Design Step I

Optimal design step I designs the laminated silicon steel sheet shape of the iron cores by using the experimental design method coupled with 2-D finite element analysis. Secondary tooth height h_p, magnet magnetization h_{pm}, air gap tilt angle θ_1, and air gap tilt angle θ_2 are selected as the design variables, which define the whole shape of the motor with the assumption

TABLE II
SELECTED FACTORS AND THEIR CORRESPONDING LEVEL FOR STEP I

Level \ Factor	A(θ_1)	B(θ_2)	C(h_p)	D(h_{PM})
1	0°	0.55	5mm	2mm
2	15°	0.6	6mm	3mm
3	30°	0.65	7mm	4mm
4	45°	0.7	8mm	5mm

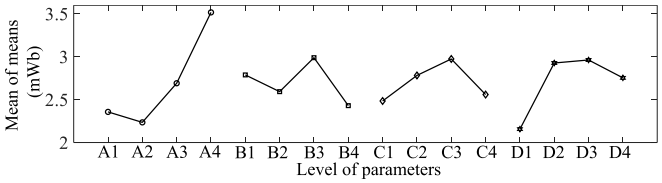

Fig. 4. Mean response of the optimal design step I.

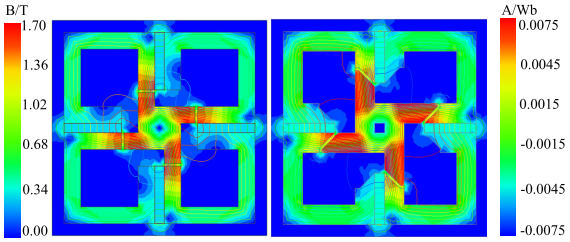

Fig. 5. Flux density distribution of the initial and optimized models.

of a constant primary diameter h_s and a constant air gap length g. The depth of the 2-D FEM is 1 m. The objective function is chosen to be the maximum flux linkage per coil. The Taguchi's method with the orthogonal table $L_{16}(4^4)$ is used. The orthogonal factor level is shown in Table II. The selected factors are the design variables. To study the optimization results, the mean response of selected factors and level, which shows the influence of each factor on the objective function, is used [12]. The mean response is shown in Fig. 4, which points out that the best setting for the flux linkage is $A_4B_3C_3D_3$. The flux density distribution of the initial and optimized model produced by the PM are shown in Fig. 5. It can be seen in Fig. 5 that the optimized model has a higher flux density with less PM. The flux linkage per coil increased from 0.034 Wb to about 0.047 Wb even though no iteration is applied, which illustrates the optimization of the motor by using 2-D FEM.

C. Optimal Design Step II

Optimal design step II designs the secondary pole pitch τ_p, the ratio of secondary unit width and secondary pole pitch $k_1 = w_{pt}/\tau_p$, and the ratio of primary unit width and secondary pole pitch $k_2 = w_{st}/\tau_p$. The other parameters are obtained in optimal design step I. The experimental design method coupled with 3-D FEM is used in the optimal design step II. The objective is to decrease the cogging force in order to perceive the quality of the motor. The Taguchi's method with the orthogonal table $L_9(3^3)$ is used and the orthogonal factor level table is shown in Table III.

TABLE III

SELECTED FACTORS AND THEIR CORRESPONDING LEVEL FOR STEP II

Factor / Level	E(τ_p)	F(K_1)	G(K_2)
1	15mm	0.8	0.8
2	18mm	0.85	0.85
3	21mm	0.9	0.95

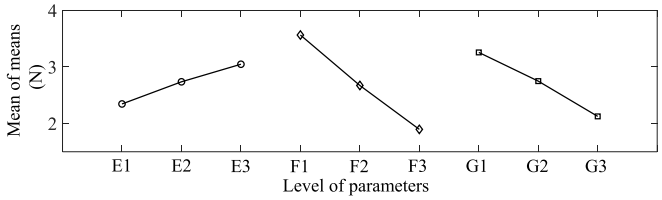

Fig. 6. Mean response of the optimal design step II.

TABLE IV

DESIGN VARIABLES VALUE OF INITIAL AND OPTIMIZED MODEL

	θ_1	θ_2	h_p	h_{pm}	τ_p	k_1	k_2
Initial	0°	0.65	6mm	4mm	15mm	0.8	0.9
Optimized	45°	0.65	7mm	4mm	15mm	0.85	0.95

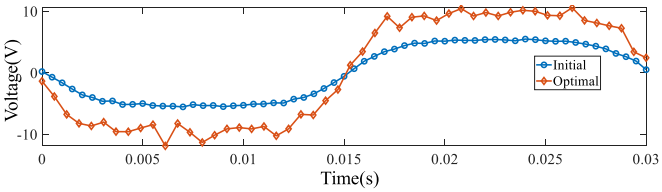

Fig. 7. No-load EMF when the mover moves at a speed of 1 m/s.

The mean response of objective is shown in Fig. 6, which points out that the best setting for the cogging force is $E_1F_3G_3$. After the optimal design step II, the optimal points of the design variables are obtained.

D. Comparison of Optimization

The optimal points of the design variables and the initial values are shown in Table IV. The magnet cost of the optimized model is decreased to about 12.5%, when compared to that of the initial model, as indicated in Tables I and IV. The no-load EMF and cogging force of both the optimized model and initial model are obtained by 3-D FEM. The comparison of no-load EMF and cogging force are separately shown in Figs. 7 and 8. The results show that the optimized motor exhibits not only higher no-load EMF but also lower cogging force as compared to the initial one. In the optimized motor, the rms no-load EMF increased from 4.4282 to 8.3927 V, and the peak cogging force reduced from 5.70 to 1.25 N, when compared to the initial motor as shown in Figs. 7 and 8. The no-load EMF of optimal model is not as smooth as the initial model because the oblique air gap structure is difficult to mesh, resulting in larger calculation error.

The motor is optimized in two steps. The second step is based on the first step. The first step is to use the 2-D FEM, which takes less time than 3-D FEM and is especially

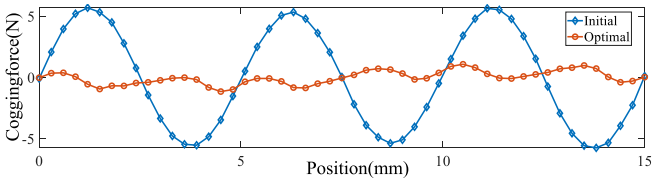

Fig. 8. Cogging force.

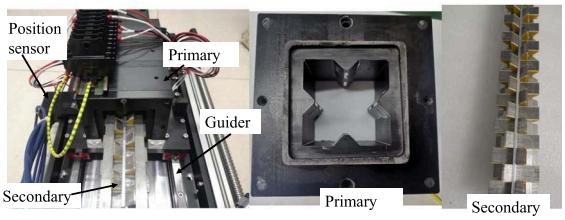

Fig. 9. Prototyped FSTFPMTLM.

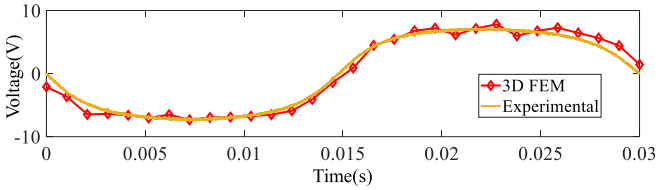

Fig. 10. EMF when the mover moves at a constant speed of 1 m/s.

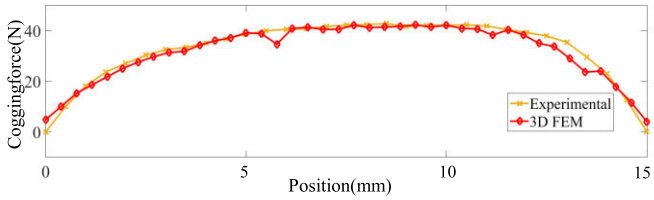

Fig. 11. Static thrust when one phase is excited with a current of 5 A.

important in the optimal design of motors, especially motors with transverse-flux structures. The two steps use different objective functions. This optimization design method reduces the optimization design time and optimizes two goals to improve the motor performance. Compared with the initial motor, the optimized one has a better performance which indicates that the proposed optimization design method is feasible.

IV. EXPERIMENTAL EVALUATION AND DISCUSSION

To validate the contribution of the proposed novel motor structure and operating principle, a prototype is manufactured. The prototyped FSTFPMTLM is shown in Fig. 9, which features a secondary unit without windings and PMs. Primary units contain PMs and windings, which are molded into a whole. Considering manufacture and magnetic saturation, the air gap length of the prototype is 1.2 mm, the magnet magnetization of the prototype is 3 mm, and the other parameters are the same as the optimized model. The EMF from the experimental and 3-D FEM when the mover moves at a constant speed of 1 m/s is shown in Fig. 10. Fig. 11 shows the static thrust from the experiment and 3-D FEM when one phase is excited with a constant current of 5 A. As shown

in Figs. 10 and 11, the ac voltage is generated when the motor is running and continuous thrust is produced when exciting different phases according to the position of the motor, indicating that the motor structure is feasible, and the principle is correct.

V. Conclusion

This article presented a novel FSTFPMTLM with the characters of simple structure, easy assembly, low air gap reluctance, low cost, and high reliability. The structure and operating principle are verified by the prototype of experimental and 3-D FEM. A two-step optimization design method is proposed for optimization of design of the novel motor. It uses the experimental design method coupled with 2-D FEM and 3-D FEM separately in different optimal design steps. Compared to the initial model of the motor, the no-load back EMF of the optimized motor increased to about 84%, the cost of PMs reduced to about 12.5%, and the peak cogging force reduced to about 78%.

Acknowledgment

This work was supported in part by the Fundamental Research Funds for the Central Universities under Grant 2020QN66.

References

[1] Q. F. Lu, Y. X. Li, X. Y. Huang, and Y. Y. Ye, "Analysis of transverse-flux linear switched-flux permanent magnet machine," *IEEE Trans. Magn.*, vol. 51, no. 11, pp. 1–4, Nov. 2015.

[2] J. Zhao, Q. Mou, K. Guo, X. Liu, J. Li, and Y. Guo, "Reduction of the detent force in a flux-switching permanent magnet linear motor," *IEEE Trans. Energy Convers.*, vol. 34, no. 3, pp. 1695–1705, Sep. 2019.

[3] R. Cao, M. Cheng, and B. Zhang, "Speed control of complementary and modular linear flux-switching permanent-magnet motor," *IEEE Trans. Ind. Electron.*, vol. 62, no. 7, pp. 4056–4064, Jul. 2015.

[4] M. Zhao *et al.*, "Development and analysis of novel flux-switching transverse-flux permanent magnet linear machine," *IEEE Trans. Ind. Electron.*, vol. 66, no. 6, pp. 4923–4933, Jun. 2019.

[5] Q. Lu, Y. Li, Y. Ye, and Y. Fang, "A novel transverse-flux switched-flux PM linear motor," in *Proc. Int. Conf. Electr. Mach. Syst. (ICEMS)*, Oct. 2013, pp. 1907–1912.

[6] Z. Zhang, X. Tang, C. Zhang, and M. Li, "Comparative study on modular longitudinal and transverse flux-switching permanent magnet linear motor," *IEEE Trans. Energy Convers.*, vol. 35, no. 1, pp. 33–42, Mar. 2020.

[7] B. Kou, J. Luo, X. Yang, and L. Zhang, "Modeling and analysis of a novel transverse-flux flux-reversal linear motor for long-stroke application," *IEEE Trans. Ind. Electron.*, vol. 63, no. 10, pp. 6238–6248, Oct. 2016.

[8] C. Liu, S. Wang, Y. Wang, G. Lei, Y. Guo, and J. Zhu, "Development of a new flux switching transverse flux machine with the ability of linear motion," *CES Trans. Electr. Mach. Syst.*, vol. 2, no. 4, pp. 384–391, Dec. 2018.

[9] D. Fu, J. Gong, Y. Xu, F. Gillon, and N. Bracikowski, "Coupled circuit and magnetic model for a transverse flux permanent magnet linear motor," *IEEE Access*, vol. 8, pp. 159274–159283, 2020.

[10] H. Chen, R. Nie, and W. Yan, "A novel structure single-phase tubular switched reluctance linear motor," *IEEE Trans. Magn.*, vol. 53, no. 11, pp. 1–4, Nov. 2017.

[11] J.-S. Shin, R. Watanabe, T. Koseki, and H.-J. Kim, "Transverse-flux-type cylindrical linear synchronous motor using generic armature cores for rotary machinery," *IEEE Trans. Ind. Electron.*, vol. 61, no. 8, pp. 4346–4355, Aug. 2014.

[12] S. Rahmatia, A. A. Tanjung, O. N. Samijayani, and W. N. Tanjung, "Network planning optimization of long term evolution radio transmitter using Taguchi's method," in *Proc. Int. Conf. Smart Comput. Electron. Enterprise (ICSCEE)*, Jul. 2018, pp. 1–6.